AIAA 2004-1819

Carbon Fibre Reinforced Plastic Tape Springs

J.C.H. Yee , O. Soykasap , and S. Pellegrino
University of Cambridge, Cambridge, CB2 1PZ, UK

45th AIAA/ASME/ASCE/AHS/ASC Structures, Structural Dynamics, and Materials Conference
19-22 April 2004
Palm Springs, CA

Carbon Fibre Reinforced Plastic Tape Springs

J.C.H. Yee*, Ö. Soykasap†, and S. Pellegrino‡
University of Cambridge, Cambridge, CB2 1PZ, UK

A tape spring is a thin-walled, straight strip of material with curved cross-section. Metallic tape springs have been used for many years, but the current trend is towards tape springs made of carbon fibre reinforced plastic (CFRP), for their tailorable properties, low mass and low coefficient of thermal expansion. The moment-rotation behaviour of a tape spring can be described as linear-elastic for small rotations and constant-moment for large rotations. Simple analytical expressions for fully characterizing this response, for a general tape spring made of CFRP, are presented in the paper and the accuracy of these expressions is assessed by means of detailed, non-linear finite-element analysis.

Introduction

A tape spring is a thin-walled, straight strip of material with curved cross-section such as, for example, a length of steel tape measure. Metallic tape springs, typically made of beryllium-copper or high-strength steel, have been used for many years as components of deployable spacecraft structures [1], but the current trend towards simpler, cheaper and more reliable deployable structures is pushing towards tape springs made of carbon fibre reinforced plastic (CFRP), which will potentially offer tailorable performance, low mass, and low coefficient of thermal expansion, as well as integral construction with other parts of a deployable structure. An example of tape springs that are manufactured as an integral part of a CFRP deployable boom has recently been investigated. [2]

A tape spring can be folded either in the *same, or equal sense*, or in the *opposite sense*. Here equal sense indicates that the bent tape spring has the same convexity as the straight one, see Fig. 1(a); in this case the edges of the tape spring are subject to compressive stresses. Conversely, opposite-sense indicates that the bent tape spring has opposite convexity to the bent one, Fig. 1(b), in which case the edges of the tape spring are subject to tensile stresses.

When an initially straight tape spring is subject to gradually increasing equal and opposite end rotations, initially it takes a uniform longitudinally curved shape. Its moment-rotation relationship is linear for sufficiently small rotations. If the tape spring is subject to opposite-sense bending, as the end rotations are increased the tape spring suddenly snaps and forms an elastic fold that is approximately straight in the transverse direction and has approximately uniform longitudinal curvature, Fig. 1(b). Then, if the rotations are further increased, the arc-length of the fold increases while its curvature remains constant.

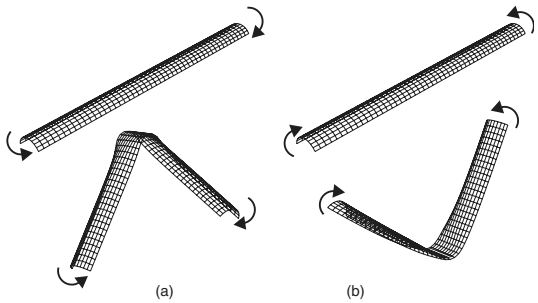

Fig. 1 Two ways of folding a tape spring: (a) equal-sense bending and (b) opposite sense bending.

If, however, the tape spring is subject to equal-sense bending, it deforms by gradually twisting over two adjacent, but separate regions whose lengths grow until the two folds merge into a single, localised fold, Fig. 1(a). Once this single fold has formed, further increasing the end rotation results —again— only in an increase of the arc-length of the fold region.

Important characteristics of this behaviour are that: (i) the elastic folds for both senses of bending have a longitudinal radius of curvature that is independent of the end rotations imposed on the ends of the tape spring; (ii) the peak stresses and strains in a folded tape spring are largely independent of the end rotations imposed on the ends; (iii) upon unfolding a tape spring snaps back into the straight configuration, this is most noticeable for a tape spring that has been bent in the opposite sense. This last characteristic makes tape springs ideal as self-latching components in deployable structures.

This paper is concerned with the design of tape springs constructed from a small number of CFRP layers. In particular, it focuses on tape springs made from woven prepregs, i.e. each layer is made from a thin carbon-fibre fabric. A methodology for the design such tape springs is established; this involves simple analyt-

*Research Student, Department of Engineering, Trumpington Street. Member AIAA.
†Research Associate, Department of Engineering, Trumpington Street. Member AIAA.
‡Professor of Structural Engineering, Department of Engineering, Trumpington Street. Associate Fellow AIAA.

ical expressions for preliminary design, whose validity is verified by means of detailed finite-element simulations.

The paper is presented in six sections. Following the present Introduction, the section Material Properties establishes the bending strain limits for thin plates made of woven CFRP, for different matrix materials. The section Behaviour of Tape Springs presents analytical expressions for the opposite-sense maximum moment that can be applied to a tape spring, and for the uniform moments associated with its folded configuration. The radius of curvature of the elastic fold and the corresponding peak fibre strains are also estimated. The section Tape Spring Design compares different tape spring designs, including single-ply triaxial prepregs and non-symmetric lay-ups, and also considers the effect of varying the angle subtended by the cross-section of the tape spring. The section Finite Element Simulations uses detailed simulations of a number of tape springs to validate the simple analytical estimates. A Discussion concludes the paper.

Material Properties

The tape springs considered in this paper are made of plain-weave T300 carbon fibre combined with different epoxy resin systems, namely 913, 914, M36, and LTM45, and also with a thermoplastic matrix, PEI; they have a fibre content between 48% and 60%. A triaxial weave T300 carbon fibre, SK802, with the 913 epoxy resin system is also considered. These fabrics are made from bundles (tows) of either 1000 or 3000 filaments, hence they will be denoted as T300-1K or T300-3K, respectively.

Plain weave fabric, see Figure 2, consists of a set of parallel, longitudinal (warp) tows and a set of transverse tows (fill) at 90° that pass alternately under and over the longitudinal tows. This is the most common weave style, and this material is the the most readily available. Its symmetrical and balanced properties, coupled with good stability and reasonable porosity, make it suitable for tape spring manufacture.

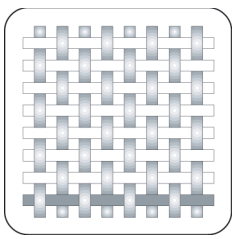

Fig. 2 Plain-weave style (source: SP Systems, 2002).

A schematic cross-section of a plain weave laminate is shown in Figure 3, where h and L are the amplitude of the wave formed by the centreline of the fibres and its wave length. Images of the cross-section of biaxial

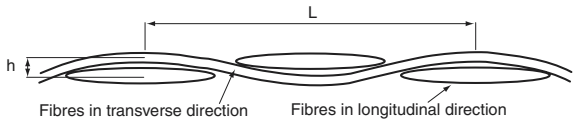

Fig. 3 Basic definitions of laminate microstructure.

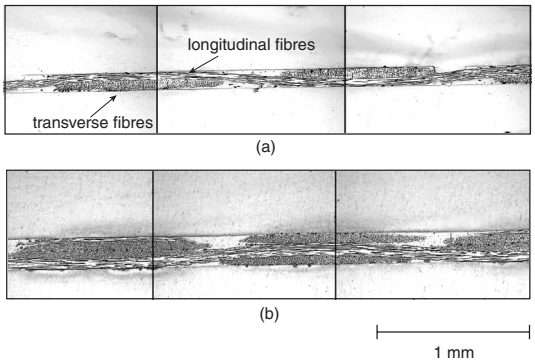

Fig. 4 Microstructure of (a) one-ply T300/913 and (b) two-ply T300/913 laminates.

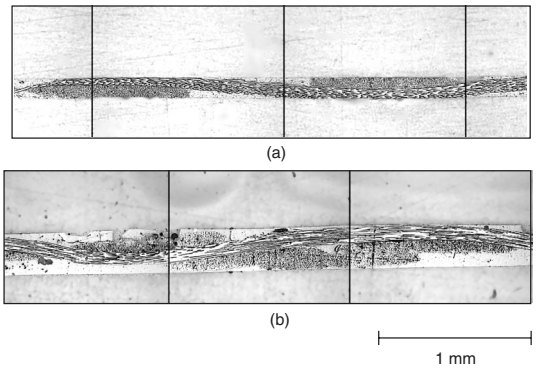

Fig. 5 Microstructure of (a) one-ply SK802/913 and (b) two-ply SK802/913 laminates.

and triaxial-weave laminates, obtained with an optical microscope, are shown in Figure 4 and Figure 5.

Yee and Pellegrino [3] have shown that these laminates are able to survive larger bending strains than the ultimate failure strains that are measured from standard coupon tests in pure tension or compression. The reason is that the standard model for laminates, classical lamination theory (CLT), [4] assumes the fibres and the matrix to be uniformly distributed in each lamina, but it is clear from Figures 4 and 5 that thin laminates made from fabrics in fact consist of bundles of fibres that are typically much thinner than the overall thickness of the laminate. Therefore, classical lamination theory needs to be used with great care in the present case (if is not altogether abandoned, in favour of a detailed micromechanical model).

The most direct approach is to model these laminates with CLT, but to determine maximum equivalent surface strains from bending tests. Details on

Table 1 Maximum bending strains in fibre dircetion

Laminate Type $[0°, 90°]$	one-ply ϵ (%)	two-ply ϵ (%)	3-ply ϵ (%)
T300-1K/PEI	2.56±0.09	2.39±0.03	1.70±0.17
T300-1K/M36	1.86±0.05	1.92±0.04	1.73±0.13
T300-1K/913	2.47±0.03	1.64±0.05	-
T300-3K/913	2.74±0.05	1.89±0.09	-
T300-3K/914	2.77±0.02	2.19±0.11	-
T300-1K/LTM45 [5]	3.01	1.93	1.82

Laminate Type $[\pm 45°]$	one-ply ϵ (%)	two-ply ϵ (%)	3-ply ϵ (%)
T300-1K/PEI	2.46±0.06	1.65±0.02	1.48±0.09
T300-1K/M36	2.02±0.12	1.70±0.05	1.42±0.03
T300-1K/913	1.97±0.04	1.24±0.03	-
T300-3K/913	2.29±0.02	1.77±0.03	-
T300-3K/914	2.64±0.03	1.79±0.04	-
T300-1K/LTM45 [5]	2.65	1.78	1.62

Laminate Type $[0°, \pm 60°]$	one-ply ϵ (%)	two-ply ϵ (%)
SK802/913	2.37±0.04	2.41±0.04

these tests can be found in Reference [3].

A summary of the maximum bending strains measured for the aforementioned composite materials is given in Table 1. For a $[0°, 90°]$ laminate, T300-1K/LTM45 can tolerate the largest strain for one-ply and 3-ply laminates, whilst T300-1K/PEI leads in the two-ply category. On the other hand, for $[\pm 45°]$ laminates, T300-1K/LTM45 has the greatest strains in all cases. Although one can observe that the maximum bending strain in plain-weave laminates decreases when the number of plies increases, this does not happen in the case of triaxial-weave laminates, where there is an insignificant difference between the maximum strains obtained from one- and two-ply specimens.

Behaviour of Tape Springs

Figure 6 shows details of a tape spring. The tape spring has initial tape radius R, initial subtended angle θ, and thickness t. The longitudinal fold radius will be denoted by r.

A schematic moment-rotation relationship for a tape spring is shown in Figure 7. Starting from the unloaded, straight configuration, for opposite sense bending the tape behaves linearly up to a maximum moment, M_{+}^{max}, or for equal sense bending down to a minimum moment, M_{-}^{*}. For rotations beyond those that correspond to these extreme values, the tape behaves as a constant moment spring, carrying M_{+}^{*} for opposite sense bending or M_{-}^{*} for equal sense bending.

Initial Behaviour

An analytical expression for the relationship between opposite-sense moment and curvature of a tape spring made of isotropic material was first obtained by Wuest [6]. Wuest considered a tape spring loaded

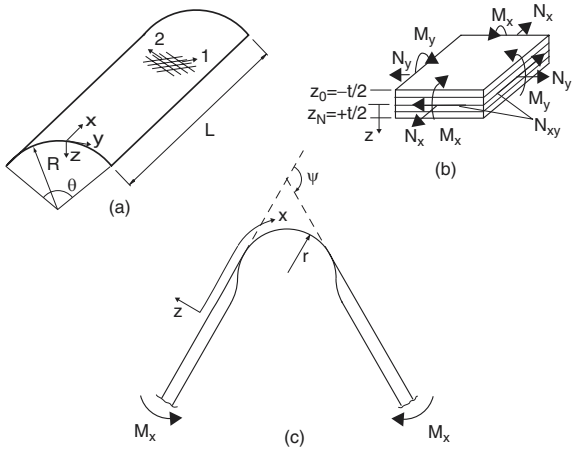

Fig. 6 Tape spring: (a) before folding, (b) ply lay-up definition, (c) equal sense folding.

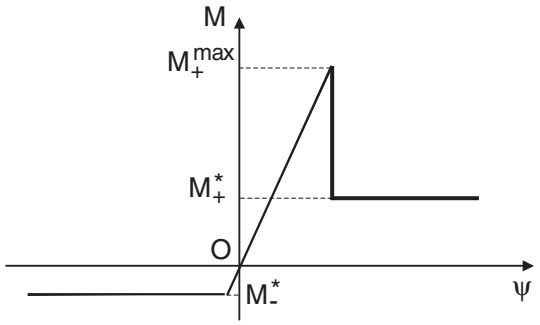

Fig. 7 Schematic moment-rotation relationship for a tape spring.

by end moments M_x that impose a *uniform* longitudinal curvature $\kappa_x = 1/r$, and determined the moment-curvature relationship for a slightly distorted axi-symmetric cylindrical shell. Wuest's relationship is extended here to include the effects of orthotropic material properties.

The constitutive equations for a thin plate, in terms of stress and strain resultants are

$$\left\{ \begin{array}{c} N \\ \dots \\ M \end{array} \right\} = \left[\begin{array}{c|c} A & B \\ \dots & \dots \\ B & D \end{array} \right] \left\{ \begin{array}{c} \epsilon^0 \\ \dots \\ \kappa \end{array} \right\} \qquad (1)$$

The off-diagonal terms in the matrix A will be neglected for simplicity, and it will be assumed that the matrix B vanishes.

The bending moments per unit length for the curvature changes κ_x, κ_y, and $\kappa_{xy} = 0$ are

$$M_x = D_{11}\kappa_x + D_{12}\kappa_y \qquad (2)$$

$$M_y = D_{12}\kappa_x + D_{22}\kappa_y \qquad (3)$$

The curvature changes in the deformed configuration of the tape are

$$\kappa_x = \frac{1}{r} \qquad (4)$$

$$\kappa_y = \frac{1}{R} - \frac{d^2w}{dy^2} \tag{5}$$

where w is the out-of-plane deflection of the deformed tape, in the z-direction. Substituting Eqs. 4 and 5 into Eqs. 2 and 3

$$M_x = D_{11}\frac{1}{r} + D_{12}\left(\frac{1}{R} - \frac{d^2w}{dy^2}\right) \tag{6}$$

$$M_y = D_{12}\frac{1}{r} + D_{22}\left(\frac{1}{R} - \frac{d^2w}{dy^2}\right) \tag{7}$$

Next, consider the differential equation of equilibrium

$$\frac{d^2M_y}{dy^2} - \frac{N_x}{r} = 0 \tag{8}$$

where N_x is the normal force per unit length, and

$$N_x = \frac{-A_{11}w}{r} \tag{9}$$

Substituting Eqs. 8 and 9 into Eq. 7 yields a fourth order ordinary differential equation

$$\frac{d^4w}{dy^4} + 4n^4\frac{w}{r^4} = 0 \tag{10}$$

where $n = \sqrt[4]{A_{11}/(4D_{22}r^2)}$. The solution of Eq. 10 is obtained by using hyperbolic functions multiplied by trigonometric functions, as follows

$$w = c_1 \cosh\frac{ny}{r}\cos\frac{ny}{r} + c_2 \sinh\frac{ny}{r}\sin\frac{ny}{r} \tag{11}$$

where c_1 and c_2 are constants to be determined by the use of the following boundary conditions. The shear force S_y and the bending moment M_y are equal to zero along the edges of the tape

$$S_y = \frac{dM_y}{dy} = 0 \quad \text{for} \quad y = \pm\frac{s}{2} \tag{12}$$

$$M_y = 0 \quad \text{for} \quad y = \pm\frac{s}{2} \tag{13}$$

where $s = 2R\sin(\theta/2)$. The constants c_1 and c_2 are

$$c_{1,2} = \mp\frac{r^2}{2n^2}\left(\frac{1}{R} + \beta\frac{1}{r}\right)\frac{\cosh\frac{ns}{2r}\sin\frac{ns}{2r} \mp \sinh\frac{ns}{2r}\cos\frac{ns}{2r}}{\cosh\frac{ns}{2r}\sinh\frac{ns}{2r} + \cos\frac{ns}{2r}\sin\frac{ns}{2r}} \tag{14}$$

where $\beta = D_{12}/D_{22}$.

The end moment, M_e, is then obtained by integrating moments about the y-axis

$$M_e = \int_{-s/2}^{s/2}(M_x + N_x w)dy \tag{15}$$

Thus,

$$\begin{aligned} M_e = \quad & sD_{11}\left[\tfrac{1}{r} + \tfrac{\beta}{R} - \beta\left(\tfrac{1}{R} + \tfrac{\beta}{r}\right)F_1\right. \\ & \left. + \left(1 + \tfrac{\beta R}{r}\right)^2 \tfrac{r}{R^2}F_2\right] \end{aligned} \tag{16}$$

where

$$F_1 = \tfrac{2}{\lambda}\tfrac{\cosh\lambda - \cos\lambda}{\sinh\lambda + \sin\lambda}$$

$$F_2 = \tfrac{F1}{4} - \tfrac{\sin\lambda\sin\lambda}{(\sinh\lambda + \sin\lambda)^2}$$

$$\lambda = \tfrac{ns}{r}$$

The maximum moment, M_+^{max}, is obtained by maximizing M_e with respect to r.

Folded Tape Spring

Analytical predictions that characterise the fold region in a tape spring can be obtained by observing that the fold region is approximately cylindrical, i.e. the transverse radius of curvature in the fold region is zero. The following analysis is more general than the analysis in the previous section, as it applies also to non-symmetric laminates.

Equation 1 can be converted to the mixed form

$$\begin{Bmatrix} \epsilon^0 \\ \cdots \\ M \end{Bmatrix} = \begin{bmatrix} A^* & \vdots & B^* \\ \cdots & & \cdots \\ C^* & \vdots & D^* \end{bmatrix} \begin{Bmatrix} N \\ \cdots \\ \kappa \end{Bmatrix} \tag{17}$$

where

$$\begin{aligned} [A^*] &= [A]^{-1} \\ [B^*] &= -[A]^{-1}[B] \\ [C^*] &= [B][A]^{-1} \\ [D^*] &= [D] - [B][A]^{-1}[B] \end{aligned}$$

Assuming that the in-plane stress resultants are negligible, i.e. $N = 0$, we obtain the mid-plane strains ϵ^0 and bending moments as follows

$$\epsilon^0 = B^*\kappa \tag{18}$$

$$M = D^*\kappa \tag{19}$$

The folded tape undergoes curvature changes, in the longitudinal and transverse directions, given by

$$(\Delta\kappa_x, \Delta\kappa_y) = (\mp\frac{1}{r}, \frac{1}{R}) \tag{20}$$

where the positive and negative signs in the first term correspond to equal and opposite sense bending, respectively. The corresponding bending moments can then be obtained from the curvature changes

$$M_x = D_{11}^*\kappa_x + D_{12}^*\kappa_y \tag{21}$$

$$M_y = D_{12}^*\kappa_x + D_{22}^*\kappa_y \tag{22}$$

The total bending strain energy over the area of the fold region, $Rr\psi\theta$, is

$$U = \frac{R\psi\theta}{2}\begin{bmatrix} \Delta\kappa_x & \Delta\kappa_y \end{bmatrix}\begin{bmatrix} M_x \\ M_y \end{bmatrix} \tag{23}$$

Substituting Eqs. 20 to 22 into Eq. 23, and minimizing the total bending energy with respect to r yields

the following expression for the radius of the fold region

$$r = \sqrt{\frac{D_{11}^*}{D_{22}^*}} R \tag{24}$$

The steady-state moments for equal and opposite sense bending of a tape spring are thus obtained by substituting Eqs. 24 and 20 into Eq. 21, and multiplying by the arc length of the tape, $R\theta$

$$M_+^* = (\sqrt{D_{11}^* D_{22}^*} + D_{12}^*)\theta \tag{25}$$

$$M_-^* = (-\sqrt{D_{11}^* D_{22}^*} + D_{12}^*)\theta \tag{26}$$

The longitudinal and transverse strains in the fold region are then obtained from CLT

$$\begin{aligned} \epsilon_x &= \epsilon_x^0 + z\kappa_x \\ \epsilon_y &= \epsilon_y^0 + z\kappa_y \end{aligned} \tag{27}$$

where, substituting Eqs. 18 and 20 into Eq. 27,

$$\begin{aligned} \epsilon_x &= \mp\frac{B_{11}^*}{r} + \frac{B_{12}^*}{R} \mp \frac{z}{r} \\ \epsilon_y &= \mp\frac{B_{12}^*}{r} + \frac{B_{22}^*}{R} + \frac{z}{R} \end{aligned} \tag{28}$$

Here, the positive and negative signs in the first and third terms on the left hand side of the equation for ϵ_x and in the first term on the left hand side of the equation for ϵ_y correspond to equal and opposite sense bending, respectively.

Tape Spring Design

This section is concerned with the design of a tape spring that has a specified moment-rotation response, defined by Figure 7, while having a sufficient margin against material failure. The design parameters include the tape radius R, the subtended angle θ, the thickness t, and the ply orientation.

Typical material properties for the laminates that have been considered in this study are given in Table 2. Note that $E_1 = E_2$, because we are dealing with plain weave and triaxial cloths, and so it follows that all laminates have equal extensional stiffness $A_{11} = A_{22}$ and also equal bending stiffness $D_{11} = D_{22}$. Then, $D_{11}^* = D_{22}^*$, and so Eq. 24 yields $r = R$.

Table 2 Material properties

Material	$E_1 = E_2$ (GPa)	G_{12} (GPa)	ν_{12} -
T300-1K/LTM45	56	3	0.05
T300-3K/913	46	4.5	0.065
SK802/913	30	10	0.5

The initial behavior of the tape spring in opposite sense bending can be obtained from Eq. 16, and depends on both material properties and the dimensions of the tape.

Figure 8 shows the effect of varying the subtended angle for a two-ply laminate, $[0°, 90°]_2$ made of T300-3K/913, while maintaining the arc length of the cross-section constant and equal to $R\theta = 14$ mm; the thickness of this laminate is 0.42 mm. The characteristic tape spring behavior for opposite-sense bending, involving a sudden snap accompanied by the formation of an elastic fold, requires the moment-curvature relationship to have an up-down-up shape, see [7] for a full explanation. Note that when the subtended angle is less than 40° for this particular laminate, the tape spring behaves practically as a flat plate.

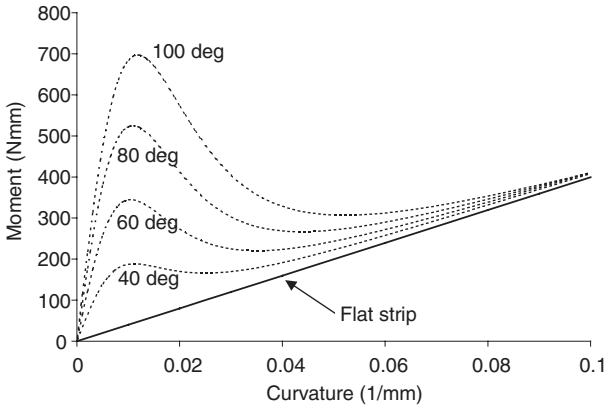

Fig. 8 Moment-curvature relationship for different subtended angles.

A lower bound for the bending stiffness of all of these constant arc-length strips is obtained by considering an initially flat strip. The initial stiffness can be easily estimated by assuming that the cross section of the tape spring does not change shape. In this case, it will have a stiffness of $E_{fx} I_{yy}$, in which E_{fx} is the flexural modulus along the x-axis and I_{yy} is the second moment of area of the cross-section about the neutral axis. These stiffness bounds are shown in Figure 9 for a tape with a subtended angle of 80°. Note that the initial stiffness is tangent to the actual behavior at $\kappa_x = 0$.

Tables 3 and 4 compare the steady-state moments of different tape springs designs, made of plain weave T300-1K/LTM45 and triaxial SK802/913, and all with a subtended angle $\theta = 100°$. The analytical estimates in the tables are listed along with results of a finite element analysis which will be detailed in the next section. Note that the two sets of results are in excellent agreement. Note that changing the ply angle in these laminates does not affect M_+^*, but affects M_-^* significantly.

The column ϵ_f in these tables lists the maximum bending strains in the fibre directions, obtained from the finite element analysis. Also note that in the laminate $[\pm 45°/0°, 90°]$ the $\pm 45°$ ply is on the inner face of the tape spring; this tape spring has lower strain levels than the alternative configuration $[0°, 90°/\pm 45°]$,

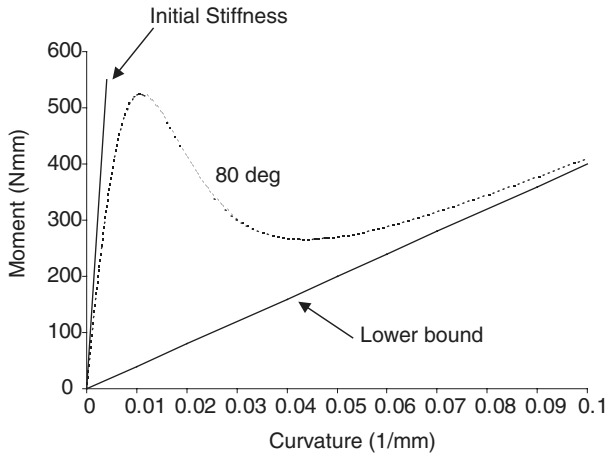

Fig. 9 Limits for moment versus curvature for $\theta = 80°$.

where the $\pm 45°$ ply is on the outer face of the tape spring, for bending in both senses.

Table 3 Steady moment M_+^*

Laminate	R (mm)	ϵ_f (%)	t (mm)	Eq.25 (Nmm)	ABAQUS (Nmm)
$*[0,90]_2$	20	0.69	0.22	91.3	94.7
$*[0,90/\pm 45]$	20	0.66	0.22	91.3	92.8
$*[\pm 45/0,90]$	15	0.79	0.22	91.3	85.2
$*[\pm 45/0,90]$	17	0.70	0.22	91.3	85.8
$*[\pm 45/0,90]$	18	0.67	0.22	91.3	87.1
$*[\pm 45/0,90]$	20	0.63	0.22	91.3	92.3
$*[\pm 45]_2$	20	0.61	0.22	91.3	87.8
Triax, 1 ply	20	0.47	0.13	19.2	20.8
Triax, 2 plies	20	0.92	0.26	153.4	151.2

*T300-1K/LTM45

Table 4 Steady moment M_-^*

Laminate	R (mm)	ϵ_f (%)	t (mm)	Eq.26 (Nmm)	ABAQUS (Nmm)
$*[0,90]_2$	20	0.88	0.22	82.6	81.1
$*[0,90/\pm 45]$	20	0.64	0.22	24.0	26.3
$*[\pm 45/0,90]$	15	0.62	0.22	24.0	23.7
$*[\pm 45/0,90]$	17	0.58	0.22	24.0	23.7
$*[\pm 45/0,90]$	18	0.57	0.22	24.0	24.2
$*[\pm 45/0,90]$	20	0.52	0.22	24.0	26.3
$*[\pm 45]_2$	20	0.44	0.22	9.3	11.2
Triax, 1 ply	20	0.60	0.13	6.4	7.6
Triax, 2 plies	20	0.94	0.26	51.1	52.2

*T300-1K/LTM45

Table 5 shows a comparison of maximum moments M_+^{max} of different tape springs made of plain weave T300-3K/913. The analytical estimates in the table, obtained by maximizing Eq. 16, are listed along with results of a finite elements analysis. When compared to the analytical approach, the finite element results are always higher. This is because Eq. 16 assumes an infinitely long tape, and so neglects the effects of the boundary conditions imposed on the ends of the tape, whereas the finite element model assumes a tape of finite length and some rigidity at the ends is required to apply the end moments.

Table 5 Maximum moment M_+^{max}

Laminate	R (mm)	θ (deg)	t (mm)	Analytical (Nmm)	ABAQUS (Nmm)
$*[\pm 45]$	20	70	0.21	44	65
$*[\pm 45]$	20	100	0.21	92	122
$*[\pm 45]_2$	20	70	0.42	260	403
$*[\pm 45]_2$	20	100	0.42	440	790

*T300-3K/913

Effect of Subtended Angle

A sensitivity study has been carried out on tape springs made of T300-3K/913, with the geometry defined in Table 6. In all cases, a total rotation of 180° of one end of the tape spring with respect to the other end was imposed. The characteristic tape-spring behaviour, in which the strains localise in a uniformly curved region, requires that the angle θ subtended by the cross-section be sufficiently large to trigger this type of behaviour. The critical angle depends on the interaction between out-of-plane bending and in-plane stretching of the laminate, as well as on the degree of anisotropy of the tape spring.

By varying the subtended angle, we can find a value above which r becomes independent of θ. The maximum strain along the fibres is compared in Table 7 with analytical estimates from Equation 28.

The variation of the radius of curvature at the centre of the tape spring, and the peak tensile and compressive strains are presented in Table 8. For one-ply $[\pm 45°]$ and two-ply $[\pm 45°]_2$, the transverse radius r gradually tends towards the value given by Equation 24. The corresponding strains, however, exceed the analytical strains when the tape spring is subjected to opposite-sense bending. This is due to edge effects which have not been addressed in this paper.

Table 6 Geometry of tape springs

Tape spring length, L	150 mm
Transverse radius, R	20 mm
Subtended angle, θ	variable (deg)
Thickness, t	
one-ply $[\pm 45°]$	0.205 mm
two-ply $[\pm 45°]_2$	0.415 mm

Table 7 Analytical predictions of maximum strains (%) in one-ply $[\pm 45°]$ tape spring

Bending Mode	Location	ϵ_x	ϵ_y	ϵ_f
Equal-sense	$+t/2$	-0.51	0.51	0.0
	$-t/2$	0.51	-0.51	0.0
Opposite-sense	$+t/2$	0.51	0.51	0.51
	$-t/2$	-0.51	-0.51	-0.51

Finite Element Simulations

Detailed simulations of the folding of a single tape spring were carried out with the ABAQUS [8] package. Both one-ply and two-ply tape springs were analysed,

Table 8 Fold radii and maximum strains

Laminate	Bending Mode	θ (deg)	r, FE (mm)	ϵ_f, FE (%)
one-ply	Opposite	70	23.8	-0.52, 0.51
$[\pm 45^\circ]$	sense	80	23.2	-0.53, 0.52
		90	22.8	-0.54, 0.53
		100	22.6	-0.55, 0.53
		110	22.3	-0.56, 0.53
		120	22.1	-0.57, 0.53
	Equal	70	21.0	-0.35, 0.31
	sense	80	20.9	-0.37, 0.34
		90	20.8	-0.39, 0.37
		100	20.7	-0.41, 0.39
		110	20.6	-0.42, 0.41
		120	20.7	-0.44, 0.43
two-ply	Opposite	70	25.9	-0.99, 0.98
$[\pm 45^\circ]_2$	sense	80	25.0	-1.01, 1.00
		90	24.4	-1.04, 1.02
		100	23.8	-1.06, 1.04
		110	23.4	-1.08, 1.05
		120	23.3	-1.10, 1.06
	Equal	70	21.7	-0.56, 0.50
	sense	80	21.4	-0.62, 0.56
		90	21.2	-0.66, 0.60
		100	21.0	-0.70, 0.65
		110	20.9	-0.73, 0.68
		120	20.8	-0.76, 0.72

and the linear-elastic material properties of Table 2 were assumed.

Element Choice

Thin shell elements were used to model the tape springs. ABAQUS offers several shell elements, and preliminary runs were carried out with 4-node quadrilateral full integration general purpose elements (S4); these elements have six degrees of freedom at each node. 4-node reduced integration shell elements (S4R5) with five degrees of freedom per node were also investigated. Eventually, the latter element was adopted, as it performs well for large rotations with only small strains. Furthermore, it uses reduced integration with hourglass control to prevent shear locking. It is also considered to be computationally economical and possesses high accuracy in modelling shell structures, as long as is not significantly distorted in plane.

A typical mesh for a tape spring depends on the subtended angle, θ. The ratio between the transverse and longitudinal length is 1:10. This is to eliminate any end effects.

Simulation Techniques

Multiple point constraints (*MPC*) were used to define the boundary conditions. The nodes on either end of the tape spring were tied to a *MPC* node, located at the centroid of the end cross section, through rigid beam elements. The main reason for locating the *MPC* nodes at the centroid is because the structure will be under pure bending when rotations are applied at the ends.

A geometrically non-linear (*NLGEOM) incremental analysis was carried out using the Newton-Raphson solution method, with automatic stabilization provided through the STABILIZE function. This solution option automatically introduces pseudo-inertia and pseudo-viscous forces at all nodes when an instability is detected. Instead of continuing with the standard quasi-static analysis, ABAQUS automatically switches to a pseudo-dynamic integration of the equations of motion for the structure, thus avoiding numerical singularities. The pseudo viscous forces are calculated based on the model's response in the first increment of the analysis step, by assuming that the dissipated energy is a fraction of the strain energy during the first step. This fraction is known as *damping intensity*, which has a default value of 2×10^{-4}. To attain accurate results, it is desirable to set this parameter to the lowest value where convergence is still achieved. In most of the analyses presented in this paper the damping intensity was set to 1×10^{-8}.

Results

Figure 10 shows a series of snapshots from the folding sequence of a one-ply $[\pm 45^\circ]$ T300/913 tape spring with $R = 20$ mm and $\theta = 90^\circ$. The tape is subjected to opposite-sense bending under monotonically increasing end rotations of the two MPC nodes.

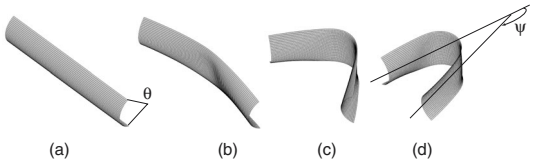

Fig. 10 Folding sequence of tape spring subject to opposite sense bending.

Figure 11 and Figure 12 show contour plots of the principal strains, for opposite-sense and equal-sense bending of this tape spring, respectively. Only the top surface strains are shown, as the distribution on the opposite surface is essentially identical but with the sign reversed. This implies that the mid-plane normal strains are negligible in this case. Note that both sets of strains are uniform through the central part of the tape spring, corresponding to the fold region. This confirms that this region is uniformly curved.

Figure 13 shows contour plots of the strain distribution along the $+45^\circ$ fibres, for opposite-sense and equal-sense bending of the tape spring. The largest strain, of around -0.61% occurs when the tape spring is subjected to opposite-sense bending. In Figure 13(a), relatively large tensile strains occur in two small regions on either side of the fold. There are only two such regions, instead of four, because we are considering the strains along one particular set of fibres.

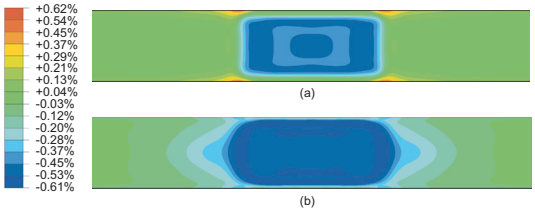

Fig. 11 Principal strains on surface $z = -t/2$ of one-ply $[\pm 45^\circ]$ tape spring under opposite-sense bending; (a) maximum strain, ϵ_x; (b) minimum strain, ϵ_y.

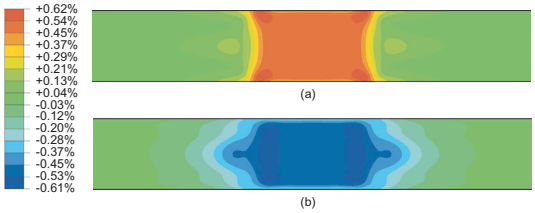

Fig. 12 Principal strains on surface $z = -t/2$ of one-ply $[\pm 45^\circ]$ tape spring under equal-sense bending; (a) maximum strain, ϵ_x; (b) minimum strain, ϵ_y.

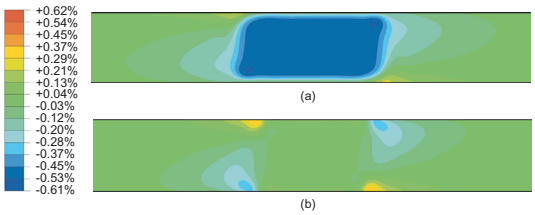

Fig. 13 Strains along $+45^\circ$ fibres, on surface $z = -t/2$ of one-ply $[\pm 45^\circ]$ tape spring for (a) opposite-sense bending and (b) equal-sense bending.

In the case of equal-sense bending, Figure 13(b), the strain in the central part of the fold region is small and the maximum strains occur in the localised strain regions on either side of the fold. Note that these peak strains are about half the maximum strains for opposite-sense bending, and so need not be considered in the design of the tape spring.

To conclude, it is interesting to consider the detailed moment-rotation plot obtained from the ABAQUS simulation, shown in Figure 14. Note that the tape spring behaves in an approximately linear-elastic way for rotations $\psi < 20.5^\circ$; at $\psi = 20.5^\circ$ a peak moment of 217 Nmm is reached. The tape spring then suddenly softens, as its deformation becomes localised at a fold, reaching a moment of ≈ 50.3 Nmm, which remains constant over a large range of ψ. If the direction of ψ is reversed, i.e. the tape spring is subjected to equal-sense bending, the tape spring response is again initially approximately linear, but this time the limit moment is lower, -92 Nmm, at a rotation $\psi = -6^\circ$. Subsequently, the tape spring softens, reaching a moment of -10 Nmm at $\psi = -27^\circ$.

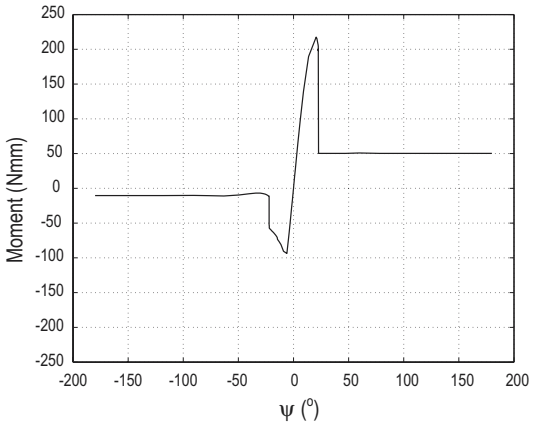

Fig. 14 Moment-rotation plot for one-ply $[\pm 45^\circ]$ T300/913.

Conclusions

The key elements for the design of woven carbon-fibre-reinforced-plastic tape springs have been established in this paper. The main headlines are as follows:

- Because these tape springs are made from one to three plies of woven carbon fibre, and the carbon fibre fabric itself consists of flattened bundles of between 1000 and 3000 fibres, a homogeneous plate model of this laminate is only acceptable if the strain limits along the fibre directions are set according to the experimentally determined values in Table 1.
- The maximum opposite-sense bending moment that can be carried by a tape spring prior to snapping is conservatively estimated by maximising Eq. 16.
- The (longitudinal) radius of the fold region in a tape spring whose cross-section subtends a sufficiently large angle is approximately the same for equal- and opposite-sense folds and can be estimated from Eq. 24.
- The steady-state moments for equal and opposite sense bending of a folded tape spring are given by Eqs. 25 and 26, respectively.
- The maximum longitudinal and transverse (principal) strains can be estimated from Eq. 28, and the corresponding strains along the fibres can then be obtained by a strain transformation.

Acknowledgments

Financial support from the Cambridge-MIT Institute (CMI), Corpus Christi College, Cambridge and QinetiQ Ltd is gratefully acknowledged. Materials and production facilities have been made generously

available by Mr John Ellis of Hexcel Ltd, Duxford. We thank Mr Glyn Dando and Dr Alan Freeman of QinetiQ Ltd for providing additional specimens and for helpful discussions.

References

[1]Rimrott, F.P.J., Storable tublar extendible member: a unique machine element. *Machine Design*, 37, 156-163, 1965.

[2]Yee, J.C.H, and Pellegrino, S., CFRP tape hinges, submitted to Journal of Aerospace Engineering, 2004.

[3]Yee, J.C.H, and Pellegrino, S., Folding of Composite Structures, DFC7 International Conference on Deformation of Fracture of Composite, Sheffield University, 22-26 April 2003.

[4]Gibson, R.F., Principles of Composite Material Mechanics, McGraw-Hill Book Co., Singapore, 1994.

[5]Gerngross, T., Folding of Thin-Walled Composite Structures, Technical University of Munich, Munich TUM-MW 65/0331-SA, 2003.

[6]Wuest,W., Einige Anwendungen der Theorie der Zylinderschale, *Z. angew. Math. Mech*, 34, 444-454, 1954.

[7]Seffen, K.A., and Pellegrino, S.. Deployment Dynamics of Tape-Springs, Proceedings of the Royal Society of London, A, 455, 1003-1048, 1999.

[8]ABAQUS, Inc., ABAQUS Theory and Standard User's Manual, Version 6.4, Pawtucket, RI, USA, 2001.